



## Controlling the Furuta pendulum: Proof of concept through virtual prototyping

L. R. C. Moura<sup>a</sup> • M. A. F. Montezuma<sup>a</sup> • M. Mendonça<sup>a</sup> •  
R. H. C. Palácios<sup>a</sup> • C. R. A. Oliveira<sup>a</sup> • A. N. Vargas<sup>a</sup> • M. A. Diop<sup>b</sup> • R. Breganon<sup>c\*</sup>

<sup>a</sup>Universidade Tecnológica Federal do Paraná, Cornélio Procópio, Paraná, Brazil

<sup>b</sup>Université Gaston Berger, Saint-Louis, Senegal

<sup>c</sup>Instituto Federal do Paraná, Jacarezinho, Paraná, Brazil

Received 10 05 2023; accepted 02 14 2024

Available 06 30 2024

**Abstract:** Furuta pendulum is a mechanism with two rotating arms. One arm rotates in the horizontal plane, while the other rotates freely in the vertical plane. The arm rotating in the vertical plane acts as an inverted pendulum. Controlling the Furuta pendulum is challenging because the underlying mechanism is highly nonlinear, unstable, and underactuated. How to control the Furuta pendulum effectively motivates this study. The main contribution of this paper is to revisit a linear control strategy that seems to stabilize the Furuta pendulum. This paper revisits the Euler-Lagrange formulation and shows how to use this formulation to represent the Furuta pendulum's nonlinear dynamics. Data from simulating the Furuta pendulum through equations and virtual prototyping suggest the effectiveness of the linear control.

**Keywords:** Furuta pendulum, linear control systems, Euler-Lagrange formulation, mechatronic systems

\*Corresponding author.

E-mail address: [ricardo.breganon@ifpr.edu.br](mailto:ricardo.breganon@ifpr.edu.br) (R. Breganon).

Peer Review under the responsibility of Universidad Nacional Autónoma de México.

## 1. Introduction

The mechatronic device known as the Furuta pendulum was devised by Furuta and colleagues in 1991—their findings were first reported in the paper by Furuta et al. (1991). In this paper, Furuta and colleagues brought attention to their novel pendulum, showing its usefulness for education in control engineering. Since then, the Furuta pendulum has become a popular expression, representing a pendulum with two rotary arms, as depicted in Figure 1.

As can be seen in Figure 1, the Furuta pendulum mechanism has two degrees of freedom. Indeed, the mechanism contains three main parts: base, horizontal arm, and vertical arm (i.e., pendulum). The base hosts a direct-current (DC) motor that produces rotational movement in the arm. On one of its sides, the horizontal arm remains attached to the motor's rod. On the other side, the horizontal arm is attached to the vertical arm, which in turn produces the pendulum movement, see Furuta et al. (1991), Zabihifar et al. (2020), Hazem et al. (2020) for further details on the construction of the Furuta pendulum. The Furuta pendulum has been studied not only in control education (Galan et al., 2019; Alves et al., 2022), but also in applications such as aerospace (Shoyama et al., 2021), robotics (Hofer & D'Andrea, 2018), and underwater vehicles (Duecker et al., 2018).

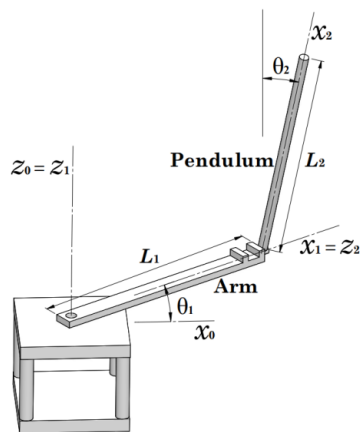


Figure 1. The Furuta pendulum with its coordinate system.

Motivated by the fact that the Furuta pendulum is nonlinear, unstable, and underactuated, researchers have become interested in developing different strategies to control and stabilize its mechanism. Plenty of studies have documented control for the Furuta pendulum. For instance, a study has proposed the so-called active disturbance rejection control to diminish undesirable effects of nonlinearities in the system response (Ramírez-Neria et al., 2014).

Another study has introduced a control based on feedback linearization, which is taken from the position and velocity

error functions (Aguilar-Avelar & Moreno-Valenzuela, 2015). In Moreno-Valenzuela et al. (2016), the authors have presented an adaptive neural network control, showing numerical evaluations for PID with neural networks. The authors of Cruz et al. (2017) show an exhaustive procedure that determines the controller gains through all possible gain combinations, picking the controller that generates the best system response. The study of Pujol-Vazquez et al. (2018) presents a magnetic device that allows the arm of the Furuta pendulum to work with  $H^\infty$  control. In Zhang and Dixon (2021), a non-minimum state feedback controller is presented with the anti-windup integrator to stabilize the Furuta pendulum. A recent study shows the control of the Furuta pendulum via a sliding mode control (SCM), illustrating the benefits of SMC for decreasing vibrations in the underlying mechanism (Nguyen et al., 2020). In Dwivedi et al. (2017), the fractional order PID controller is developed using a control parameter adjustment technique through gain margin, phase margin, and Nyquist graph; the application of this technique improves the robustness of the controller. The approach of Yang and Zheng (2018) shows trajectory planning so that the pendulum oscillates from its downright position to its upright position; this task is accomplished through the adaptive neural network with linear matrix inequalities. What the research from these papers taken together suggests is that the control of the Furuta pendulum remains a challenge.

The main contribution of this paper is to show simulation data from a virtual prototype Furuta pendulum. This prototype worked with the classical linear quadratic regulator with integral action (LQR+I) control during the simulations. To adjust the LQR+I parameters, we use the pendulum's model, as usual in the literature (Ramírez-Neria et al., 2014). Note that the pendulum's model can be obtained from both the Euler-Lagrange formulation Cazzolato and Prime (2011), Fantoni and Lozano (2002) and Kane's method Hamza et al. (2019)—the dynamics from both methods coincide. Even though the Euler-Lagrange formulation has been covered in the literature Cazzolato and Prime (2011), Fantoni and Lozano (2002), we decided to revisit it here using virtual prototyping to reliably validate the mathematical modeling of a complex system, in this case, the Furuta pendulum. Where it is possible to identify whether the simplifications in the model don't differ too much from the model created through virtual prototyping that doesn't have these simplifications and consumes less time to be made. And suggest a reference (Moura, 2021) on which this paper is based that presents the development of mathematical modeling using the Euler-Lagrange method, explaining a greater number of steps and considerations regarding them that facilitate the understanding of the application of the methodology. Another important point was that the coordinate system that referenced the links was positioned using Denavit-Hartenberg's parameters, as in the

coordinate systems that reference the links, the z-axis is positioned according to the degree of freedom of the joint and the x according to the length of the link which makes it easier to know where the parameters  $\alpha_{i-1}$ ,  $a_{i-1}$ ,  $d_i$  e  $\theta_i$  are as shown in Figure 2.

An interesting conclusion from our simulated data is that the LQR+I control seems to stabilize the Furuta pendulum. Namely, we simulate the Furuta pendulum in two distinct ways: (i) nonlinear dynamics from the Euler-Lagrange formulation and (ii) virtual prototyping designed in the Adams software (Newport Beach, California, USA). The simulated data from both models suggest that the Furuta pendulum is stable under the LQR+I control. This numerical evidence emphasizes the potential of the LQR+I control for stabilizing the Furuta pendulum.

**Remark 1:** To the best of the authors' knowledge, there is no proof that the LQR+I control stabilizes the Euler-Lagrange model representing the Furuta pendulum. No formal proof is available.

Our conclusion that the LQR+I control seems to stabilize the Furuta pendulum only comes from observing simulated data. Yet it is worth emphasizing that no definitive conclusion about stability can be drawn only from simulated data.

This paper is organized as follows. Section 2 presents the Euler-Lagrange modeling of the Furuta pendulum and its main parameters. Section 3 shows the linear control strategy and the corresponding simulated data. Finally, Section 4 presents some concluding remarks.

**Notation:** The symbol  $\mathbb{R}^n$  denotes the  $n^{th}$  dimensional Euclidean space. The superscript  $T$  on  $U^T$  denotes the transpose when  $U$  represents either a vector or matrix. The operator  $diag(a_1, \dots, a_n)$  defines the diagonal matrix of dimension  $\mathbb{R}^{n \times n}$  comprising the elements  $a_1, \dots, a_n$  arranged in its main diagonal. We borrow from Cazzolato and Prime (2011) the notation that defines the dynamics of the Furuta pendulum.

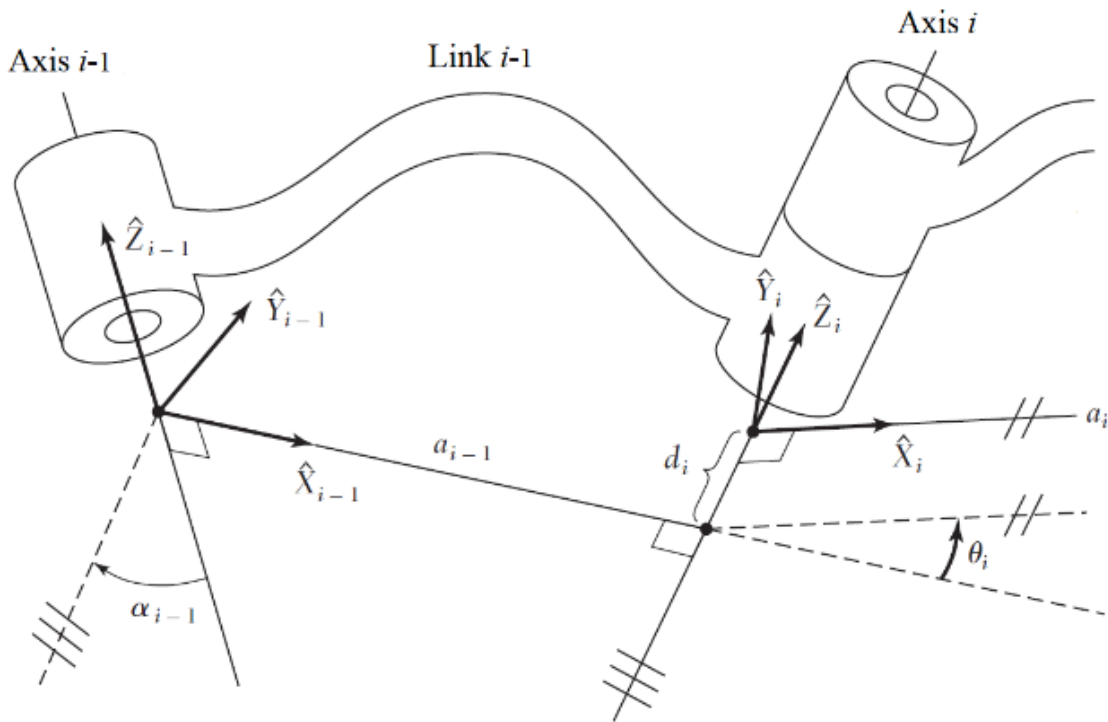


Figure 2. Connection of two subsequent links according to Denavit-Hartenberg (Craig, 2005).

## 2. Dynamics of the Furuta pendulum

Recall that the ‘control goal’ of the Furuta pendulum is to balance its pendulum in the inverted position through torque control. The torque must be applied to keep the angle  $\theta_2$  as close as possible to zero, i.e., driving the arm  $L_2$  to the vertical position (see Figure 1). To generate this torque, we rely on a DC motor that rotates the arm  $L_1$  around the axis  $Z_0$ , thus generating the angle  $\theta_1$ . While increasing or decreasing  $\theta_1$ , the DC motor keeps applying torque  $\tau_1$  upon the arm  $L_1$ . The arm  $L_2$  moves freely because its joint with  $L_1$  has no actuator. As in Cazzolato and Prime (2011), we assume that  $m_1$  and  $m_2$ , located at  $\ell_1$  and  $\ell_2$ , represent the mass of the two arms. The two arms are damped by the constants  $b_1$  and  $b_2$ .

Next, we present the Euler-Lagrange formulation that represents the dynamics of the Furuta pendulum.

### 2.1. Euler-Lagrange formulation: Nonlinear dynamics for the Furuta pendulum

Next, we use the notation borrowed from Craig (2005) [Ch. 2 and 6] to represent the system of coordinates of the Furuta pendulum.

Let us denote the fixed coordinate system by  $\{0\}$ . As indicated in Figure 1, the coordinate systems are  $\{0\}$ ,  $\{1\}$  and  $\{2\}$ , and they correspond to  $(x_0, y_0, z_0)$ ,  $(x_1, y_1, z_1)$ , and  $(x_2, y_2, z_2)$ , respectively. The coordinate system  $\{0\}$  shows the initial position of the arm. The coordinate system  $\{1\}$  shows the displacement performed on the arm. The coordinate system  $\{2\}$  shows the pendulum's observed displacement due to the arm's displacement. More details are given below.

The coordinate system  $\{1\}$  moves with the arm. To the displacement of the arm, the z-axis  $\{0\}$  is rotated for  $\theta_1$ . To describe the pendulum's displacement, the y-axis is rotated in  $-\pi/2$  radians and moved  $L_1$  along the x-axis. The x-axis is then rotated in  $\pi$  radians. Finally, the z-axis is rotated in  $\theta_2$ . The coordinate system  $\{2\}$  moves with the pendulum itself.

Using Euler angles, we can write the rotation matrices  $R$  of the arm as (Craig, 2005, Ch. 2):

$${}^1_0R_{z'y'x'} = \begin{bmatrix} \cos(\theta_1) & \sin(\theta_1) & 0 \\ -\sin(\theta_1) & \cos(\theta_1) & 0 \\ 0 & 0 & 1 \end{bmatrix}, \quad (1)$$

and of the pendulum as:

$${}^2_1R_{y'x'z'} = \begin{bmatrix} 0 & -\sin(\theta_2) & \cos(\theta_2) \\ 0 & -\cos(\theta_2) & -\sin(\theta_2) \\ 1 & 0 & 0 \end{bmatrix}. \quad (2)$$

Following the notation of Cazzolato and Prime (2011), we denote the axial moment of inertia in the x-axis by  $I_{1x}$  for the arm and by  $I_{2x}$  for the pendulum and, respectively, by  $I_{1y}$ ,  $I_{1z}$ ,

$I_{2y}$ ,  $I_{2z}$  for the other corresponding axes (the unity of moment of inertia is  $kg \cdot m^2$ ).

Define the function  $F_1 : \mathbb{R}^6 \rightarrow \mathbb{R}$  as:

$$\begin{aligned} F_1(\theta_1, \dot{\theta}_1, \ddot{\theta}_1, \theta_2, \dot{\theta}_2, \ddot{\theta}_2) &= b_1\dot{\theta}_1 + I_{1z}\ddot{\theta}_1 + \ell_1^2 m_1 \ddot{\theta}_1 + L_1^2 m_2 \ddot{\theta}_1 \\ &- L_1 \ell_2 m_2 \ddot{\theta}_2 \cos(\theta_2) \\ &+ I_{2x} \ddot{\theta}_1 \cos^2(\theta_2) \\ &+ L_1 \ell_2 m_2 \dot{\theta}_2^2 \sin(\theta_2) + (I_{2y} \\ &+ \ell_2^2 m_2) \ddot{\theta}_1 \sin^2(\theta_2) \\ &- I_{2x} \dot{\theta}_1 \dot{\theta}_2 \sin(2\theta_2) \\ &+ I_{2y} \dot{\theta}_1 \dot{\theta}_2 \sin(2\theta_2) \\ &+ \ell_2^2 m_2 \dot{\theta}_1 \dot{\theta}_2 \sin(2\theta_2), \end{aligned} \quad (3)$$

and  $F_2 : \mathbb{R}^6 \rightarrow \mathbb{R}$  as:

$$\begin{aligned} F_2(\theta_1, \dot{\theta}_1, \ddot{\theta}_1, \theta_2, \dot{\theta}_2, \ddot{\theta}_2) &= b_2\dot{\theta}_2 + I_{2z}\ddot{\theta}_2 + \ell_2^2 m_2 \ddot{\theta}_2 \\ &- L_1 \ell_2 m_2 \dot{\theta}_1 \cos(\theta_2) - g \ell_2 m_2 \sin(\theta_2) \\ &+ (+I_{2x} - I_{2y} - \ell_2^2 m_2) \dot{\theta}_1^2 \cos(\theta_2) \sin(\theta_2). \end{aligned} \quad (4)$$

Now, we can present the main result of this section. The nonlinear dynamics of the Furuta pendulum are given by:

$$F_i(\theta_1, \dot{\theta}_1, \ddot{\theta}_1, \theta_2, \dot{\theta}_2, \ddot{\theta}_2) = \tau_i, \quad i = 1, 2. \quad (5)$$

The pendulum rotates freely. Then there is no external torque applied to it. Thus,  $\tau_2 = 0$ . That proves the underactuated system, with 2 DOF (rotation in the arm and rotation in the pendulum) and only one torque applied ( $\tau_1$  in the arm).

### 2.2. Euler-Lagrange formulation: Linearization of the Furuta pendulum dynamics

This section introduces some assumptions that allow us to convert the nonlinear dynamics of the Furuta pendulum into a linear system.

The arm and pendulum are slender rods, which means that the moments of inertia around the axes that cross the rod are equal, as suggested in Hibbeler (2010), [Appx. C5]. In addition, the moment of inertia around the axis along the rod is taken to be zero.

**Remark 2:** An immediate consequence is that  $I_{1x}$  and  $I_{2x}$  can be replaced by zero while  $I_y$  and  $I_z$  are kept equal. Thus, from now on, the terms  $Y_1$  and  $Y_2$  are used to denote  $Y_1 = I_{1y} = I_{1z}$  and  $Y_2 = I_{2y} = I_{2z}$ .

Let us introduce the following terms:

$$\begin{aligned} \Pi_1 &= Y_1 + m_1(\ell_1)^2, \\ \Pi_2 &= Y_2 + m_2(\ell_2)^2, \\ \Pi_0 &= Y_1 + m_1(\ell_1)^2 + m_2(L_1)^2, \end{aligned}$$

where  $\Pi_1$  and  $\Pi_2$  relate the center of mass of the arm and its point of rotation (arm and pendulum, respectively); the term  $\Pi_0$  relates the overall system to the DC motor rotation point, as suggested in Hibbeler (2010), [Ch. 10].

These simplifications allow us to linearize the nonlinear dynamics (5), as detailed next. It is necessary to rewrite (5) to obtain the angular accelerations and consequently enable linearization.

$$\begin{bmatrix} \ddot{\theta}_1 \\ \ddot{\theta}_2 \end{bmatrix} = \begin{bmatrix} \Pi_0 + \Pi_2 \sin^2(\theta_2) & -L_1 \ell_2 m_2 \cos(\theta_2) \\ -L_1 \ell_2 m_2 \cos(\theta_2) & \Pi_2 \end{bmatrix}^{-1} \times \left( \begin{bmatrix} -b_1 - \Pi_2 \dot{\theta}_2 \sin(2\theta_2) & -L_1 \ell_2 m_2 \dot{\theta}_2 \sin(\theta_2) \\ \frac{1}{2} \Pi_2 \dot{\theta}_1 \sin(2\theta_2) & -b_2 \end{bmatrix} \begin{bmatrix} \dot{\theta}_1 \\ \dot{\theta}_2 \end{bmatrix} + \begin{bmatrix} \tau_1 \\ g \ell_2 m_2 \sin(\theta_2) \end{bmatrix} \right) \quad (6)$$

With linearization, we want to obtain the linear representation in state-space:

$$\dot{\mathbf{x}} = \mathbf{A}\mathbf{x} + \mathbf{B}\mathbf{u} \quad (7)$$

where  $\mathbf{A} \in \mathbb{R}^{n \times n}$  is the state matrix,  $\mathbf{x} \in \mathbb{R}^n$  is the vector of states,  $\mathbf{B} \in \mathbb{R}^{n \times r}$  is the input matrix, and  $\mathbf{u} \in \mathbb{R}^r$  is the vector of input. Set:

$$\mathbf{x} = [\theta_1 \quad \theta_2 \quad \dot{\theta}_1 \quad \dot{\theta}_2]^T \in \mathbb{R}^4, \quad \text{and} \quad \mathbf{u} = \tau_1 \in \mathbb{R} \quad (8)$$

The linearization of (5) is done using the Jacobian matrix method, when  $\theta_1 = 0$ ,  $\theta_2 = 0$ ,  $\dot{\theta}_1 = 0$ ,  $\dot{\theta}_2 = 0$ , and  $\tau_1 = \tau$ . The matrices obtained are:

$$\mathbf{A} = \begin{bmatrix} 0 & 0 & 1 & 0 \\ 0 & 0 & 0 & 1 \\ 0 & \frac{g L_1 \ell_2^2 m_2^2}{\Pi_0 \Pi_2 - L_1^2 \ell_2^2 m_2^2} & \frac{-b_1 \Pi_2}{\Pi_0 \Pi_2 - L_1^2 \ell_2^2 m_2^2} & \frac{-b_2 L_1 \ell_2 m_2}{\Pi_0 \Pi_2 - L_1^2 \ell_2^2 m_2^2} \\ 0 & \frac{g \Pi_0 \ell_2 m_2}{\Pi_0 \Pi_2 - L_1^2 \ell_2^2 m_2^2} & \frac{-b_1 L_1 \ell_2 m_2}{\Pi_0 \Pi_2 - L_1^2 \ell_2^2 m_2^2} & \frac{-b_2 \Pi_0}{\Pi_0 \Pi_2 - L_1^2 \ell_2^2 m_2^2} \end{bmatrix} \quad (9)$$

and

$$\mathbf{B} = \begin{bmatrix} 0 \\ 0 \\ \frac{\Pi_2}{\Pi_0 \Pi_2 - L_1^2 \ell_2^2 m_2^2} \\ \frac{L_1 \ell_2 m_2}{\Pi_0 \Pi_2 - L_1^2 \ell_2^2 m_2^2} \end{bmatrix} \quad (10)$$

### 2.3. Virtual prototyping of the Furuta pendulum

A prototype of the Furuta pendulum was developed in SolidWorks (Waltham, Massachusetts, USA), see Figure 3.

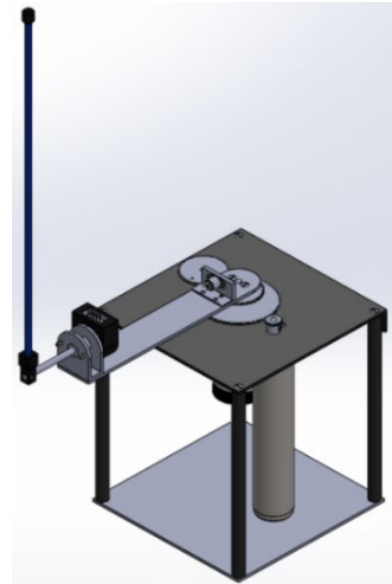


Figure 3. Furuta pendulum prototype developed in SolidWorks.

The prototype features were extracted from SolidWorks, see Table 1. These features were later transferred to the virtual prototyping software Adams (Newport Beach, California, USA) because Adams can emulate the real-time dynamics of a Furuta pendulum.

Table 1. Features of the Furuta Pendulum.

Symbol	Value	Unity
$L_1$	0.21600	m
$\ell_1$	0.07735	m
$m_1$	0.25700	kg
$L_2$	0.33700	m
$\ell_2$	0.16375	m
$m_2$	0.12700	kg
$I_{1x}$	0.000147009	kg m <sup>2</sup>
$I_{1y}$	0.001405289	kg m <sup>2</sup>
$I_{1z}$	0.001503506	kg m <sup>2</sup>
$I_{2x}$	0.000025630	kg m <sup>2</sup>
$I_{2y}$	0.001594099	kg m <sup>2</sup>
$I_{2z}$	0.001618580	kg m <sup>2</sup>
$Y_1$	0.001503506	kg m <sup>2</sup>
$Y_2$	0.001618580	kg m <sup>2</sup>
$b_1, b_2$	0	N/m/s

### 3. Linear state-feedback control: Numerical evaluations

We have two nonlinear models. The first was obtained by analytical calculation, and the second by virtual prototyping. For the LQR application, it is necessary to calculate the linear format of the two models. Just after, it is possible to calculate

the LQR gains. The LQR provides a multivariable proportional regulator, where it is necessary to add an integrator to the controller to eliminate steady-state errors between the reference signal and the controlled state variable, which in this case is the angular position of link 1. Therefore, the LQR control needs to have integral action. The block diagram of one LQR with the integral action, also known as LQR+I, is shown in Figure 4.

Then, we linearized the model obtained with the Euler-Lagrange formulation and configured the computational calculation to result in the linear model. Thus, we found the gains  $\mathbf{K}_1$  and  $\mathbf{K}_2$  with the linear models for both cases.

The matrices in (9) and (10) corresponding to the features in Table 1 are:

$$\mathbf{A} = \begin{bmatrix} 0 & 0 & 1 & 0 \\ 0 & 0 & 0 & 1 \\ 0 & 36.8369 & 0 & 0 \\ 0 & 73.5300 & 0 & 0 \end{bmatrix}, \quad (11)$$

$$\mathbf{B} = \begin{bmatrix} 0 \\ 0 \\ 202.016 \\ 180.625 \end{bmatrix}.$$

By virtual prototyping, the matrices are:

$$\mathbf{A} = \begin{bmatrix} 0 & -6.4e - 15 & 0 & 37.7345 \\ 1 & 0 & 0 & 0 \\ 0 & -6.3e - 15 & 0 & 74.7420 \\ 0 & 0 & 1 & 0 \end{bmatrix}, \quad (12)$$

$$\mathbf{B} = \begin{bmatrix} 205.6364 \\ 0 \\ 185.0149 \\ 0 \end{bmatrix}.$$

It is important to emphasize that the most significant values are in different positions in the two models because the states' position in the state vector differs between them.

Next, we revisit the tracking control of linear systems (Ostertag, 2011, Sec. 1.8). For a given reference signal  $\mathbf{r} \in \mathbb{R}$ , we compute the error signal, i.e.,  $\mathbf{e} = \mathbf{r} - \mathbf{y} \in \mathbb{R}$  where  $\mathbf{y} = [1 \ 0 \ \dots \ 0]\mathbf{x}$ , and  $\mathbf{x} \in \mathbb{R}^4$  satisfies (7) – (10). Define  $\mathbf{z}(t) \equiv \int_0^t \mathbf{e}(\tau) d\tau$  for all  $t \geq 0$ , and:

$$\mathbf{u} \equiv [\mathbf{K}_1 \ \mathbf{K}_2] \begin{bmatrix} \mathbf{x} \\ \mathbf{z} \end{bmatrix}. \quad (13)$$

Since  $\dot{\mathbf{z}} = \mathbf{e}$  we can write (Ostertag, 2011, Sect. 1.8.1):

$$\begin{bmatrix} \dot{\mathbf{x}} \\ \dot{\mathbf{z}} \end{bmatrix} = \begin{bmatrix} \mathbf{A} + \mathbf{BK}_1 & \mathbf{BK}_2 \\ -[1 \ 0 \ \dots \ 0] & \mathbf{0} \end{bmatrix} \begin{bmatrix} \mathbf{x} \\ \mathbf{z} \end{bmatrix} + \begin{bmatrix} \mathbf{0} \\ \mathbf{1} \end{bmatrix} r. \quad (14)$$

The control problem consists of finding the gains  $\mathbf{K}_1^T \in \mathbb{R}^4$  and  $\mathbf{K}_2 \in \mathbb{R}$  that minimizes the linear-quadratic-regulator

with the integral action (LQR+I) cost with  $\mathbf{r} \equiv \mathbf{0}$  (Anderson & Moore, 1989, Ch. 3; Rosinová & Veselý, 2006, p. 196):

$$J = \frac{1}{2} \int_0^\infty (\mathbf{x}(t)^T \mathbf{Q} \mathbf{x}(t) + \mathbf{u}(t)^T \mathbf{R} \mathbf{u}(t)) dt \quad (15)$$

It is known that the minimum value of (15) is attained when solving the usual Riccati equation (Anderson & Moore, 1989, Ch. 3). In our case, the optimal solution for the model given by (11) is:

$$\mathbf{K}_1 = [-0.5778 \ 2.5781 \ -0.2044 \ 0.3749] \quad (16)$$

and  $\mathbf{K}_2 = 0.8165$

and for the model given by (12) is:

$$\mathbf{K}_1 = [-0.2044 \ -0.5784 \ 0.3717 \ 2.5642] \quad (17)$$

and  $\mathbf{K}_2 = 0.8165$

provided that  $\mathbf{Q} = \text{diag}(0.001, 0.01, 10^{-4}, 10^{-4})$  and  $\mathbf{R} = 15$ . The values of  $\mathbf{Q}$  and  $\mathbf{R}$  were chosen by trial and error.

Now we apply the linear state-feedback control strategy (13) in three different models: (i) nonlinear dynamics as in (5); (ii) linear system as in (7) subject to (11); and (iii) virtual prototyping (Adams). We assume the initial condition  $\mathbf{x}_0 = [0 \ 0 \ 0 \ 0]^T$  for all the simulations.

We build the closed loop system of the two nonlinear models as follows. For the formulation model, the gains of equation (16) control the model shown in (5). The nonlinear model obtained with virtual prototyping is controlled through the gains of (17).

The resulting data taken from these three models are summarized in Figure 5. As can be seen, the three models generate similar responses, yet the response from the linear system seems to drift away from the other two during the transient time. As expected, the pendulum's angular position and the control action oscillate for a while and return to a steady state.

To prove the system's stability, we can mention that all the eigenvalues of the state matrix of the closed-loop augmented system contain a negative real part for the linear models. The eigenvalues of the linear model by prototyping are  $-2.5834 + 3.9166i$ ,  $-2.5834 - 3.9166i$ ,  $-9.3798 + 0.0000i$ ,  $-8.0587 + 0.0000i$ , and  $-4.1159 + 0.0000i$ . The eigenvalues of the linear model by formulation are  $-9.1022 + 0.0000i$ ,  $-8.1267 + 0.0000i$ ,  $-2.5483 + 3.9467i$ ,  $-2.5483 - 3.9467i$ ,  $-4.1014 + 0.0000i$ . The local behavior of a nonlinear system near a linearization point is very similar to the behavior of the linear system at that point. It is precisely for this reason that we use the gains obtained for linearized systems in nonlinear models. Therefore, a nonlinear system can also be considered stable close to the linearization point.

The LQR+I control showed a good performance and low control effort, similar to that presented in Hazem et al. (2020) for the double-link rotary inverted pendulum system.

**Remark 3:** The three models for the Futura pendulum were extensively simulated using distinct profiles. In all simulations, we observed that the models remained stable. This numerical evidence suggests that.

In summary, the simulated data suggest that the linear state-feedback control (13) can stabilize the three models. This numerical evidence encourages using (13) for the Furuta pendulum in real time.

**Remark 4:** A video that shows the simulation in Adams was recorded and is available freely at [https://youtu.be/w3Pg60J\\_3cM](https://youtu.be/w3Pg60J_3cM). This video illustrates the prototype of the Furuta pendulum moving its arms for distinct references according to the LQR+I control (13).

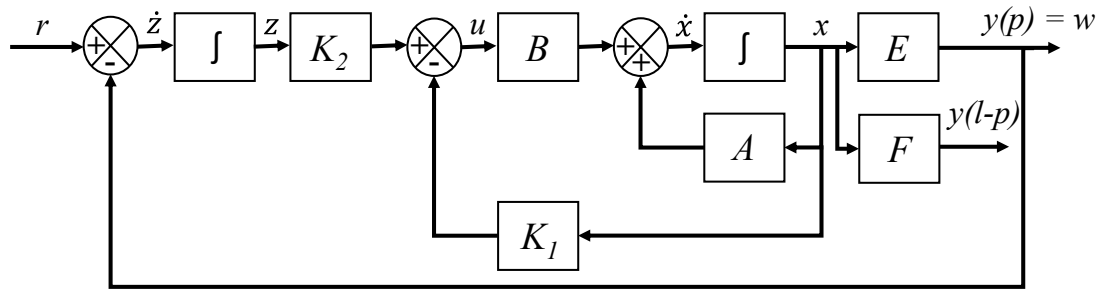


Figure 4. Block diagram for the LQR+I control (adapted from d’Azzo & Houpis, 1995).

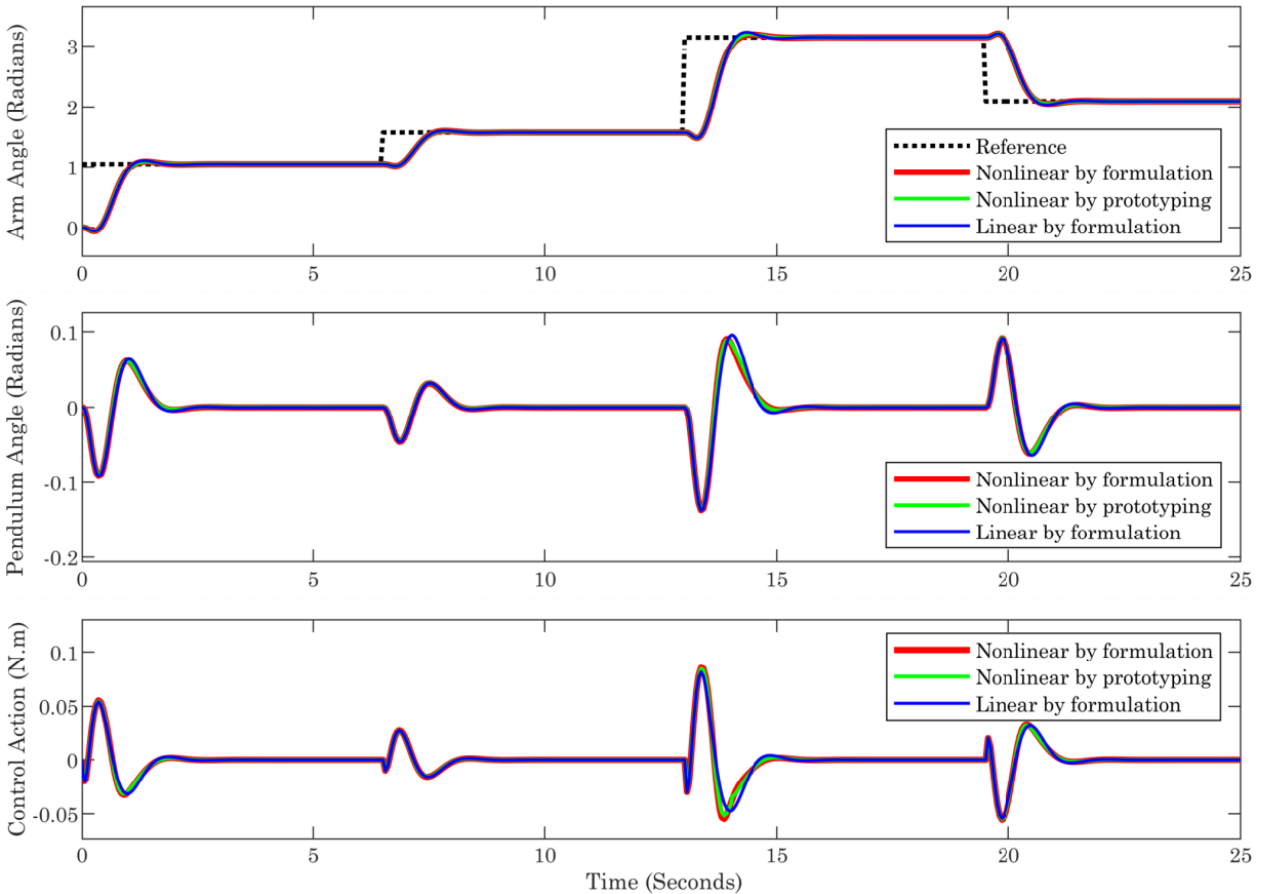


Figure 5. Simulated data. Three models were simulated with linear control (13) subject to (16).

## 4. Conclusions

This paper has revisited the modeling and control of the Furuta pendulum. This paper documents how to obtain the nonlinear dynamics of the Furuta pendulum through the Euler-Lagrange formulation, following Cazzolato and Prime (2011). The nonlinear dynamics then fed a linear model that has given rise to the linear feedback control. The linear feedback control was then applied to the nonlinear dynamics, the behavior of the nonlinear dynamics seems to agree with the one from the virtual prototyping Adams (see Section 3). Data from both models (i.e., nonlinear dynamics and virtual prototyping) suggest that the linear control can stabilize the Furuta pendulum. This fact motivates further research on how to design efficient, simple controllers to ensure the Furuta pendulum's stability. This paper, then, can be interpreted as a step in that direction.

## Conflict of interest

The authors declare that the research was conducted without any commercial or financial relationships that could be construed as a potential conflict of interest.

## Acknowledgements

The authors would like to thank the Universidade Tecnológica Federal do Paraná, Cornélio Procópio, for their support in the development of this work.

## Funding

Research supported in part by the Brazilian agencies CAPES grant 88881.030423/2013-01 and CNPq grant 305158/2017-1 and 401572/2016-1.

## References

Aguilar-Avelar, C., & Moreno-Valenzuela, J. (2015). A composite controller for trajectory tracking applied to the Furuta pendulum. *ISA transactions*, 57, 286-294. <https://doi.org/10.1016/j.isatra.2015.02.009>

Alves, U. N. L. T., Breganon, R., Pivovar, L. E., de Almeida, J. P. L. S., Barbara, G. V., Mendonça, M., & Palácios, R. H. C. (2022). Discrete-time  $H_\infty$  integral control via LMIs applied to a Furuta pendulum. *Journal of Control, Automation and Electrical Systems*, 33(3), 1-12. <https://doi.org/10.1007/s40313-021-00867-x>

Anderson, B. D.O., & Moore, J.B. (1989). *Optimal control: linear quadratic methods*. Englewood Cliffs, New Jersey, USA: Prentice Hall Inc.

Cazzolato, B. S., & Prime, Z. (2011). On the dynamics of the furuta pendulum. *Journal of Control Science and Engineering*, 2011, 1-8. <https://doi.org/10.1155/2011/528341>

Craig, J.J. (2005). *Introduction to robotics. Mechanics and control*. Upper Saddle River, NJ, USA. Pearson Prentice Hall, 3<sup>th</sup> ed.

Cruz, M. A., Ortigoza, R. S., Sánchez, C. M., Guzmán, V. H., Gutierrez, J. S., & Lozada, J. H. (2017). Parallel computing as a tool for tuning the gains of automatic control laws. *IEEE Latin America Transactions*, 15(6), 1189-1196. <https://doi.org/10.1109/TLA.2017.7932708>

d'Azzo, J. J., & Houpis, C. D. (1995). *Linear control system analysis and design: conventional and modern*. McGraw-Hill Higher Education.

Duecker, D. A., Hackbarth, A., Johannink, T., Kreuzer, E., & Solowjow, E. (2018). Micro underwater vehicle hydrobatocs: A submerged furuta pendulum. In *2018 IEEE International Conference on Robotics and Automation (ICRA)* (pp. 7498-7503). IEEE. <https://doi.org/10.1109/ICRA.2018.8461091>

Dwivedi, P., Pandey, S., & Junghare, A. S. (2017). Stabilization of unstable equilibrium point of rotary inverted pendulum using fractional controller. *Journal of the Franklin Institute*, 354(17), 7732-7766. <https://doi.org/10.1016/j.jfranklin.2017.09.013>

Fantoni, I., & Lozano, R. (2002). Stabilization of the Furuta pendulum around its homoclinic orbit. *International Journal of Control*, 75(6), 390-398. <https://doi.org/10.1080/0020717011011226>

Furuta, K., Yamakita, M., Kobayashi, S., & Nishimura, M. (1991). A New Inverted Pendulum Apparatus for Education. *IFAC Proceedings Volumes*, 25(12), 133-138. [https://doi.org/10.1016/S1474-6670\(17\)50102-0](https://doi.org/10.1016/S1474-6670(17)50102-0)

Galan, D., Chaos, D., De La Torre, L., Aranda-Escolastico, E., & Heradio, R. (2019). Customized online laboratory experiments: A general tool and its application to the furuta inverted pendulum [Focus on Education]. *IEEE Control Systems Magazine*, 39(5), 75-87. <https://doi.org/10.1109/MCS.2019.2925256>



- Hamza, M. F., Yap, H. J., Choudhury, I. A., Isa, A. I., Zimit, A. Y., & Kumbasar, T. (2019). Current development on using Rotary Inverted Pendulum as a benchmark for testing linear and nonlinear control algorithms. *Mechanical Systems and Signal Processing*, 116, 347-369.  
<https://doi.org/10.1016/j.ymssp.2018.06.054>
- Hazem, Z. B., Fotuhi, M. J., & Bingül, Z. (2020). Development of a Fuzzy-LQR and Fuzzy-LQG stability control for a double link rotary inverted pendulum. *Journal of the Franklin Institute*, 357(15), 10529-10556.  
<https://doi.org/10.1016/j.jfranklin.2020.08.030>
- Hibbeler, R.C. (2010). *Engineering Mechanics - Dynamics*, Upper Saddle River, NJ, USA: Pearson Prentice Hall.
- Hofer, M., & D'Andrea, R. (2018). Design, modeling and control of a soft robotic arm. In *2018 IEEE/RSJ International Conference on Intelligent Robots and Systems (IROS)* (pp. 1456-1463). IEEE.  
<https://doi.org/10.1109/IROS.2018.8594221>
- Moura, L. R. C. (2021). *Mathematical modeling and control of a furuta pendulum*. Dissertation (Master in Mechanical Engineering) - Universidade Tecnológica Federal do Paraná, Cornélio Procópio.
- Ramírez-Neria, M., Sira-Ramírez, H., Garrido-Moctezuma, R., & Luviano-Juarez, A. (2014). Linear active disturbance rejection control of underactuated systems: The case of the Furuta pendulum. *ISA transactions*, 53(4), 920-928.  
<https://doi.org/10.1016/j.isatra.2013.09.023>
- Nguyen, N. P., Oh, H., Kim, Y., Moon, J., Yang, J., & Chen, W. H. (2020). Fuzzy-based super-twisting sliding mode stabilization control for under-actuated rotary inverted pendulum systems. *IEEE Access*, 8, 185079-185092.  
<https://doi.org/10.1109/access.2020.3029095>
- Ostertag, E. (2011). *Mono-and multivariable control and estimation: linear, quadratic and LMI methods*. Springer Science & Business Media.
- Rosinová, D., & Veselý, V. (2006). Robust PID decentralized controller design using LMI. *IFAC Proceedings Volumes*, 39(14), 53-58.  
<https://doi.org/10.3182/20060830-2-SF-4903.00010>
- Shoyama, T., Banno, A., Furuta, Y., Kurata, N., Ode, D., Wada, Y., & Matsui, T. (2021). Air-Launch Experiment Using Suspended Rail Launcher for Rockoon. *Aerospace*, 8(10), 289.  
<https://doi.org/10.3390/aerospace8100289>
- Moreno-Valenzuela, J., Aguilar-Avelar, C., Puga-Guzmán, S. A., & Santibáñez, V. (2016). Adaptive neural network control for the trajectory tracking of the Furuta pendulum. *IEEE transactions on cybernetics*, 46(12), 3439-3452.  
<https://doi.org/10.1109/TCYB.2015.2509863>
- Pujol-Vazquez, G., Acho, L., Mobayen, S., Nápoles, A., & Pérez, V. (2018). Rotary inverted pendulum with magnetically external perturbations as a source of the pendulum's base navigation commands. *Journal of the Franklin Institute*, 355(10), 4077-4096.  
<https://doi.org/10.1016/j.jfranklin.2018.03.013>
- Yang, X., & Zheng, X. (2018). Swing-up and stabilization control design for an underactuated rotary inverted pendulum system: Theory and experiments. *IEEE Transactions on Industrial Electronics*, 65(9), 7229-7238.  
<https://doi.org/10.1109/TIE.2018.2793214>
- Zabihifar, S. H., Yushchenko, A. S., & Navvabi, H. (2020). Robust control based on adaptive neural network for Rotary inverted pendulum with oscillation compensation. *Neural Computing and Applications*, 32, 14667-14679.  
<https://doi.org/10.1007/s00521-020-04821-x>
- Zhang, L., & Dixon, R. (2020). Robust nonminimal state feedback control for a Furuta pendulum with parametric modeling errors. *IEEE Transactions on industrial Electronics*, 68(8), 7341-7349.  
<https://doi.org/10.1109/TIE.2020.3001811>